AGU PUBLICATIONS

Radio Science

RESEARCH ARTICLE
10.1002/2015RS005709

All-sky interferometric riometry

Derek McKay[1,2], Richard Fallows[3], Menno Norden[3], Anita Aikio[4], Juha Vierinen[5], Farideh Honary[6], Steve Marple[6], and Thomas Ulich[1]

[1]Sodankylä Geophysical Observatory, University of Oulu, Sodankylä, Finland, [2]Rutherford Appleton Laboratory, STFC, Didcot, UK, [3]ASTRON, ,Dwingeloo, Netherlands, [4]Department of Astronomy and Space Physics, University of Oulu, Oulu, Finland, [5]MIT Haystack Observatory, Westford, Massachusetts, USA, [6]Department of Physics, Lancaster University, Lancaster, UK

Key Points:
- The first use of all-sky interferometry for riometric imaging is presented
- Unlike multibeam riometers, interferometry allows continuous spatial sampling
- The KAIRA facility was used to produce *D* region all-sky absorption maps

Correspondence to:
D. McKay,
derek.mckay@sgo.fi

Citation:
McKay, D., R. Fallows, M. Norden, A. Aikio, J. Vierinen, F. Honary, S. Marple, and T. Ulich (2015), All-sky interferometric riometry, *Radio Sci.*, *50*, 1050–1061, doi:10.1002/2015RS005709.

Received 19 MAR 2015
Accepted 25 SEP 2015
Accepted article online 1 OCT 2015
Published online 21 OCT 2015

Abstract The first implementation of a Fourier-based *interferometric riometry* technique for measuring electron density induced ionospheric opacity at VHF radio frequencies is presented. Unlike multibeam riometers, which form discrete beams on the sky, the interferometric technique permits all-sky sampling of incoming cosmic radio noise emissions resulting in a spatially continuous radiogram of the entire sky. The map of the received power at each time may then be compared to the equivalent map from a "quiet day," allowing the morphology of ionospheric absorption of cosmic radio noise to be ascertained. In this work, the high-latitude Kilpisjärvi Atmospheric Imaging Receiver Array was used to carry out the first interferometric riometry measurements in late 2013, producing all-sky absorption maps of space-weather-related ionization in the *D* region.

1. Introduction

Detection of cosmic radio noise absorption events by the ionosphere was first demonstrated by *Shain* [1951]. The name riometer (originally: Relative Ionospheric Opacity Meter for Extra-Terrestrial Emissions of Radio noise [*Little and Leinbach*, 1959]) is commonly used to describe the instrument that measures this absorption. In the first instance, a riometer measures the power of these cosmic radio emissions. Radio waves are naturally attenuated by collisions between free electrons and neutrals, typically in the ionospheric *D* region (70–90 km) and, at times of ionospheric disturbance such as during aurorae or other particle precipitation events, increases in the electron density cause enhanced absorption of the radio signals [*Hargreaves*, 1995].

Riometers have hitherto been either single-beam or multibeam systems, typically operating with a single observing frequency in the range of 25–40 MHz. Initially, riometers were single detectors, typically with a wide antenna beam pattern, pointing toward the local zenith. This does not discriminate between the direction in which the absorption occurs but provides a single measurement point associated with the location. More general spatial information about absorption in the ionosphere can be achieved by operating multiple riometers spread out over a larger geographical region and comparing temporal lag in absorption events, such as the Finnish Riometer Chain operated by the Sodankylä Geophysical Observatory [*Ranta and Ranta*, 1977].

Variants of the single-beam riometer include fixed-zenith narrow-beam systems and narrow-beam scanning riometers. However, a more comprehensive approach is to have a so-called multibeam system [*Honary et al.*, 2011]. These multibeam riometers were developed in the 1990s [*Detrick and Rosenberg*, 1990] with additional improvements made through the use of Butler matrices or digital beam forming to synthesize different pointing directions from a fixed phased array. An example of this is the imaging riometer for ionospheric studies (IRIS) [*Browne et al.*, 1995]. Each of the beams in this system measures its own power and thus operates as a quasi-independent riometer for that pointing direction. Each beam is, in effect, a "pixel" on the sky and thus a crude image of riometric absorption can be formed. This leads to these multibeam systems being referred to as imaging riometers.

The multibeam imaging riometers allow spatial distribution of absorption to be measured in different directions but are still limited in that each beam is discrete. Thus, discontinuities between detection directions and undersampling of the spatial absorption results in uncertainties regarding the temporal movement and evolution of these events.

Figure 1. The location of Kilpisjärvi, where the KAIRA facility is sited. Also shown are the locations of Sodankylä Geophysical Observatory and Oulu University.

Recent advances in all-sky interferometry have been exploited as part of new astronomical observatories, such as the Low-Frequency Array (LOFAR) [*van Haarlem et al.*, 2013]. It was realized that the same techniques apply to the riometry case, and the existence of a LOFAR-type radio telescope at Kilpisjärvi in northern Finland would be ideally suited due to its geographical location where geomagnetic storm absorption events occur [*Ranta and Ranta*, 1977]. This facility is the Kilpisjärvi Atmospheric Imaging Receiver Array (KAIRA) [*McKay-Bukowski et al.*, 2015]. The location of Kilpisjärvi is shown in Figure 1.

This paper describes the work done using KAIRA to develop and demonstrate the first application of all-sky interferometric riometry. Section 2 describes radio interferometry and its application to riometry. It also introduces the KAIRA system and describes the experimental method used. Section 3 describes the results obtained showing that the method is sound, and section 4 provides a statistical comparison between results obtained with KAIRA with those measured by the nearby IRIS facility. Section 5 discusses the significance of the results, the challenges that are faced, and future prospects.

2. All-Sky Interferometric Riometry

Riometry is not the only method that relies on the measurement of sky radio noise. Radio astronomers have also attempted to do this using a variety of techniques. Early radio telescopes have used arrays, initially of dipole-based systems, but later of steerable parabolic-type dish antennas. This choice was driven partly by the desire to find suitable receiving systems for the frequency of scientific interest and also to improve sensitivity. These parabolic dish arrangements restrict the field of view but give greater sensitivity. Sophisticated techniques have been developed for multibeam systems, such as fan-beam synthesis as used in the Mills Cross designs [*Burke*, 1956]. This technique has been explored for the purposes of riometry, where complications due to sidelobe response [*Hagfors et al.*, 2003] were corrected using tapering. Imaging riometers to date have often been filled-aperture multibeam systems [*Honary et al.*, 2011].

However, the main drive in radio telescope design during the latter part of the 20th century has been for interferometric systems comprising multiple parabolic dishes sampling in the Fourier domain. The interferometer provides superior imaging capability and the ability to use extended baselines for improved angular resolution, while the use of parabolic dishes provides an initial beamforming stage and increased element sensitivity.

2.1. The Van Cittert-Zernike Theorem

The principle of electromagnetic interferometry was identified by van Cittert, who established that a correlation function between sampled signals in a plane is independent of whether the plane is illuminated directly or via a focusing mechanism, but rather corresponds only to the diffraction function defined by the separation of those sample points [*van Cittert*, 1934]. *Zernike* [1938] formalized this in statistical terms and defined the concept of *degree of coherence* between two points to represent the amplitude of the diffraction pattern and, by using a suitable coordinate system, expressed this using the Fourier theorem. The relationship between the source signal distribution and the covariance of the signals received at two different points (often termed as the correlation) is referred to as the van Cittert-Zernike theorem and is expressed as

$$V(u,v) = \iint I(l,m)\, e^{-2\pi i(ul+vm)}\, \mathrm{d}l\mathrm{d}m \tag{1}$$

with the terms defined and explained in the following sections.

$V(u,v)$ is the complex visibility as a function of the baseline displacement coordinates (u,v) [*Thompson*, 1999]. The more general three-dimensional differential coordinates (u,v,w) for a baseline between antennas i and j can be calculated from their positions as

$$\left.\begin{aligned} u &= (e_j - e_i)/\lambda \\ v &= (n_j - n_i)/\lambda \\ w &= (h_j - h_i)/\lambda \end{aligned}\right\} \tag{2}$$

where e, n, and h are the orthogonal topocentric coordinates of the antennas (in directions east, north, and vertically, respectively, applicable for the Northern Hemisphere) and λ is the observed radio wavelength. For the all-sky imaging described in this paper, the third dimension of the baseline displacement (namely, in the direction of the array phase center, typically notated as w) can always be set to zero, as the nominal center is in the direction of zenith and the instrument used in this experiment, KAIRA, is a level, coplanar array [*McKay-Bukowski et al.*, 2015]. Thus, the w term is omitted from equation (1).

The synthesized image expressed as the intensity $I(l,m)$ in equation (1) is a plane normal to the Zenith direction. The coordinates l and m are proportional to the sines of the angles measured from the origin of the (l,m) plane, which is coincident with zenith in the topocentric case [*Thompson*, 1999]. This is the relationship of an orthographic projection, summarized as

$$l = \sin(Z)\sin(A); \quad m = \sin(Z)\cos(A) \tag{3}$$

where A is the azimuth and Z is the zenith angle. This relationship is applicable for the Northern Hemisphere and is demonstrated in Figure 2.

The van Cittert-Zernike theorem makes assumptions about the radiation source. First, it must be incoherent in order to have a useful correlation function. Second, the electromagnetic flux must not change appreciably within the time period of the correlation. These assumptions also apply to riometry due to the constant flux of the Galactic synchrotron background and dominant radio sources at VHF frequencies (Cas A, Cyg A), although the latter can exhibit strong ionospheric scintillation at such frequencies. This ionospheric scintillation effect results in rapid fluctuation in the received radiation from these sources due to dynamic radio caustics [*Little and Lovell*, 1950; *Ryle and Hewish*, 1950].

The Sun is an occasional variable source which can dominate the radio sky at VHF frequencies and thus result in problems for the observations although, during the experiments described here, the Sun was below the horizon. Artificial radio frequency interference (RFI) can also be present, but the choice of a radio-quiet environment, coupled with the ability of the interferometric technique to readily discern directions, makes identification of artificial sources relatively straightforward.

Sampling of the (u,v) plane can be accomplished either through instantaneous sampling, or synthesis, such as reconfigurable arrays, Earth rotation aperture synthesis, or combinations of both [*Ryle et al.*, 1959]. How well the (u,v) plane is sampled, through either of these methods, is referred to as the (u,v) coverage and this term is used to qualitatively indicate what level of expected image integrity can be expected.

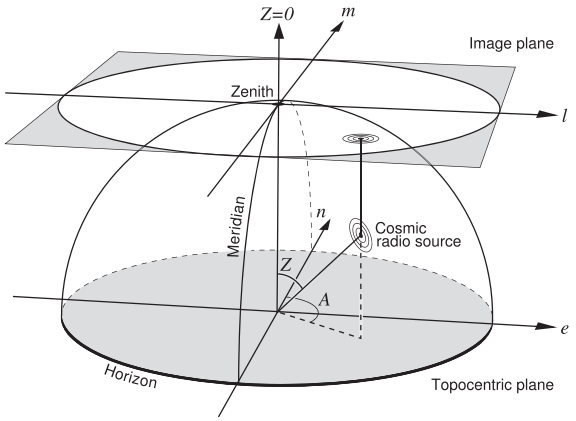

Figure 2. The association between the topocentric perspective and the (l,m) plane showing the orthographic relationship between the celestial sphere and the image plane. An example source has been placed at an arbitrary azimuth and zenith angle (A, Z).

To accomplish all-sky, high time resolution imaging, instantaneous sampling with sufficient (u,v) coverage is required. Only in recent years has it been possible to attempt this rapid all-sky imaging, through advances in digital signal processing and information network technology. The current generation of radio telescopes rely on both of these to achieve their capabilities [*van Haarlem et al.*, 2013].

The interferometric technique can also be used for riometry. Systems such as LOFAR operate in a suitable frequency range and have the benefit of nearly all-sky coverage, and have been suggested as suitable for riometry [*Hagfors et al.*, 2003]. However, until recently, there have been no such systems deployed in geographical areas where intense absorption occurs. In the domain of geophysical radio remote sensing, techniques of interferometric imaging are already widely used for imaging of coherent scatter from ionospheric irregularities (Coherent Radar Imaging, CRI, e.g., *Woodman* [1971], *Kudeki and Sürücü* [1991], and *Hysell and Chau* [2006]).

2.2. The KAIRA System

In 2011 – 2012, the first phased-array system at high latitudes, capable of Fourier interferometric all-sky radio imaging, was constructed. Called KAIRA (Kilpisjärvi Atmospheric Imaging Receiver Array), it was built as a test system for incoherent scatter radar reception; however, it has also been designated for numerous other science experiments [*McKay-Bukowski et al.*, 2015]. KAIRA comprises a dual array of omnidirectional VHF radio antennas and makes extensive use of the proven LOFAR antenna and digital signal-processing hardware [*van Haarlem et al.*, 2013].

A review of other large phased-array imaging riometers was given in *Honary et al.* [2011]. KAIRA has 48 antennas, which is less than the featured riometer in the review paper (e.g., IRIS, 64). However, the quasi-random array layout gives it superior sidelobe suppression and permits a wider separation, which results in similar field size and, thus, beam size. The arrays reviewed either rely on Butler matrix back ends or digital beamforming. KAIRA has a fully digital, polyphased, arbitrary beam controller, but KAIRA is also fitted with an interferometric correlator, which is key to the experiment described here.

For riometry, the KAIRA Low Band Antenna (LBA) array was used, as it can receive frequencies from 8 to 80 MHz, and thus receive the frequency range optimal for riometry. The LBA array center is 20.7620758°E, 69.0707445°N, and the LBAs themselves are crossed inverted-V-dipole aerials, standing 1.8 m tall, above a 3×3 m steel-grid ground plane. The antenna impedance varies from capacitive (short dipole approximation) to inductive (where the dipole is long compared to the wavelength) and is resonant at approximately 58 MHz. An inverted-V dipole is optimized for maximum sensitivity to electromagnetic fields from within zenith angles of $\pm 60°$. The dipole length is approximately 2.4 m and the wires are at a 45° angle with the vertical plastic center pole.

The antennas are scattered in a quasi-random pattern across a field approximately 34 m in diameter (Figure 3) to give a beam profile with low sidelobes. The beam size is frequency dependent and, because of the fixed

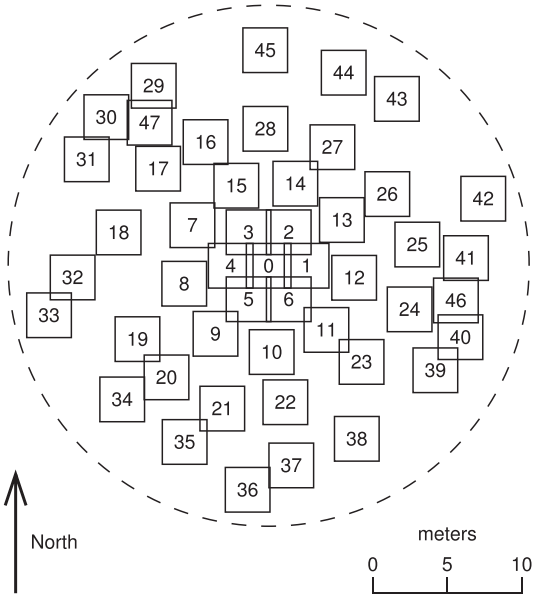

Figure 3. The KAIRA LBA array layout. The squares mark the metal ground planes of each dipole showing the physical extent of the antennas, each labeled with the antenna's identification number.

antenna locations, is subject to a sec(Z) elongation in the vertical axis for nonzero zenith angle, Z. This distortion is not apparent in the resulting images due to the orthographic projection used for the $I(l,m)$ plane.

The large number of antennas, relative to the size of the array, means that although the coverage is not complete, the (u,v) plane is nonetheless well sampled (Figure 4). Allowing for the fact that the dipoles have nonzero extent means that their contribution to the (u,v) coverage is also nonzero in area, thus resulting in a (u,v) plane that is close to being filled. This eliminates the need to carry out deconvolution (such as CLEAN, [*Högbom*, 1974]) to reconstruct the image from sparsely sampled (u,v) data.

Each polarization from each antenna is connected via coaxial cable with a receiver unit (RCU) board in a central, RF-shielded enclosure. The RCUs provide bandpass filtering and 12 bit, 200 Msample/s analog-to-digital conversion. Data transport is done using 16 bit words. A digital polyphase filter separates the signal from each RCU into 512 "subbands" with nominal spectral widths of 195.3125 kHz each.

Each subband is a dual-polarization complex signal, $\{X_{re}, X_{im}, Y_{re}, Y_{im}\}$, where X and Y are the polarization channels. In the normal 16 bit data transport mode, up to 244 of these subbands can be arbitrarily distributed

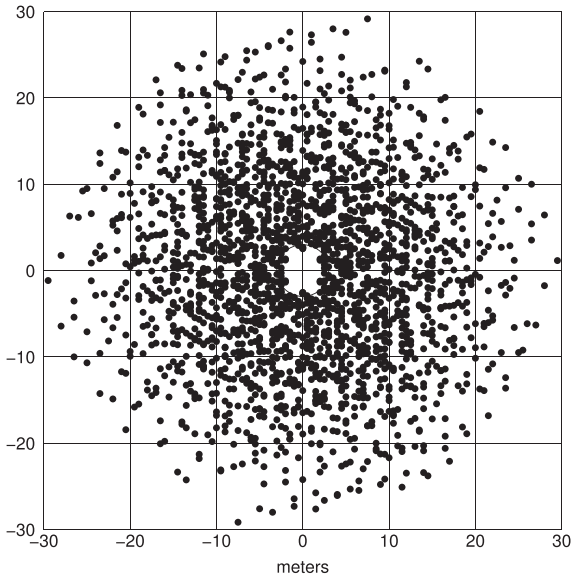

Figure 4. The instantaneous zenith (u,v) coverage provided by the KAIRA LBA array.

over the band pass, with delayed, weighted addition to provide independent beamforming. However, in the 8 bit data transport mode, 488 subbands can be selected. Each subband plus beamformed direction is referred to as a "beamlet."

KAIRA can select multiple arbitrary frequencies within the range of its broadband front ends (approximately 8–80 MHz for the LBA array). It can also form multiple beams in arbitrary directions. These features give a distinct advantage as a multidirectional spectral riometer, which none of the other facilities (all approximately 37–39 MHz) can achieve.

This has already been used to demonstrate multibeam, multifrequency riometry [*Kero et al.*, 2014]. However, the system also includes a configurable single-frequency-channel correlator which calculates the covariance matrix for all RCUs in the array for one subband each second. This can be configured to step through the 512 subbands for the purposes of calibration and monitoring, or it can be configured to continuously correlate on a single subband, which is what is used in this work to demonstrate all-sky interferometric riometry. For KAIRA, there are 48 dual-polarization antennas, resulting in a matrix of 96×96 complex powers. These values are complex, because $(a + \mathrm{i}b) \times (c - \mathrm{i}d) = ac + \mathrm{i}(bc - ad) + bd$, where $(a + \mathrm{i}b)$ is the subband sample from one antenna and $(c - \mathrm{i}d)$ is a subband sample from another antenna.

2.3. Data Acquisition and Processing

Calibration is done by applying predetermined gain, phase, and delay corrections to the input signals. This is executed as part of routine observatory operations and is not specific to the riometric interferometry experiment. Additionally, cable lengths and other engineering and configuration parameters are included automatically into the system. The corrections are applied in real time so the data are recorded precalibrated.

The ionospheric absorption is dependent on the frequency of the radio wave [*Hargreaves*, 1995]. The higher the frequency, the lower the absorption. Additionally, the source of background cosmic noise is the general haze of Galactic synchrotron emission and this drops off as a -2.55 power law with frequency [*Guzmán et al.*, 2011; *Roger et al.*, 1999]. Lower frequencies result in a complete cutoff of the radio propagation through the ionosphere and are additionally disturbed by interference from shortwave radio services. An intermediate range of approximately 20–50 MHz is best suited for the riometric technique.

The subband (≡ frequency channel) of 195 was used, which has a central frequency and channel bandwidth of 38.086 ± 0.098 MHz with a resulting beam size of approximately $15 \times 15 \sec(Z)$ degrees. This central frequency was chosen to match the IRIS instrument, which permits comparisons (see section 4). The relatively narrow bandwidth makes the interferometer approximately monochromatic and eliminates decorrelation and bandwidth-smearing effects.

The correlator was run simultaneously with KAIRA's routine multibeam riometry experiment, again to permit comparison. The correlator was configured to generate antenna covariance matrices every second and store them as records in 1 h cross-correlation statistics files [*Virtanen*, 2012]. The output data are 64 bit integers per two complex components, per RCU baseline. There are 96^2 RCU baselines recorded, including autocorrelations. The entire matrix is stored, even though RCU pairs are Hermitian; thus, a duplication of data exists. Additionally, there is no need for this experiment to record correlations between different polarizations for different antennas. These features may become useful in future experiments or for the purposes of data integrity validation. Thus, the complete matrix is recorded, resulting in a data rate of 147,456 bytes/s. These data are saved as hourly files, thus ≈531 MB per file (≈12.7 GB/d).

The exponential in equation (1) is fixed and results in a matrix of $N_{\mathrm{pixels}} \times N_{\mathrm{baselines}}$. This transform matrix for a given antenna array layout, observing frequency and resultant image pixel size, can be predetermined. Once that has been done, the transform matrix only needs to be loaded from disk which is faster, and this needs only to be done once with it being held in fast-access memory for the remainder of the processing. The dot product of this matrix with the covariance matrix is done by fast linear algebra libraries, and thus permits faster-than-real-time data processing without the need for special hardware.

As for all riometry, a quiet-sky power needs to be determined to be compared against any given all-sky image. This is done by taking the median of all data for a given position in the tangent plane (l, m) for sidereal times

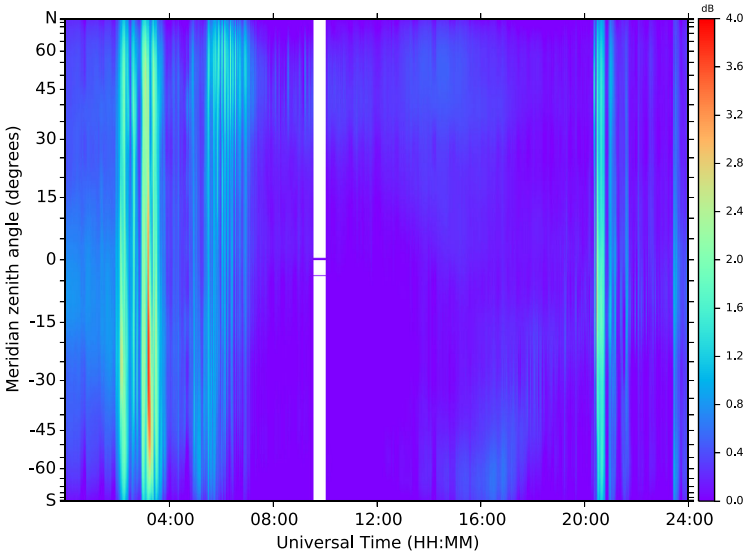

Figure 5. Interferometric riometry keogram at 38.086 MHz showing the full UT day of 2 October 2013. The meridional axis is in orthographic projection. The blank strip between 09:33 and 10:01 was when data recording was switched off.

equivalent to the sidereal time of the all-sky image, over a period of time prior to the observation. This permits determination of the amount of radio noise absorption,

$$A = 10 \log_{10}(P_q/P) \tag{4}$$

where P_q is the quiet-sky power, P is the observed power, and A is absorption in dB. For the results presented in section 3, quiet-sky power was determined from a period spanning 14 days prior to the day of the event.

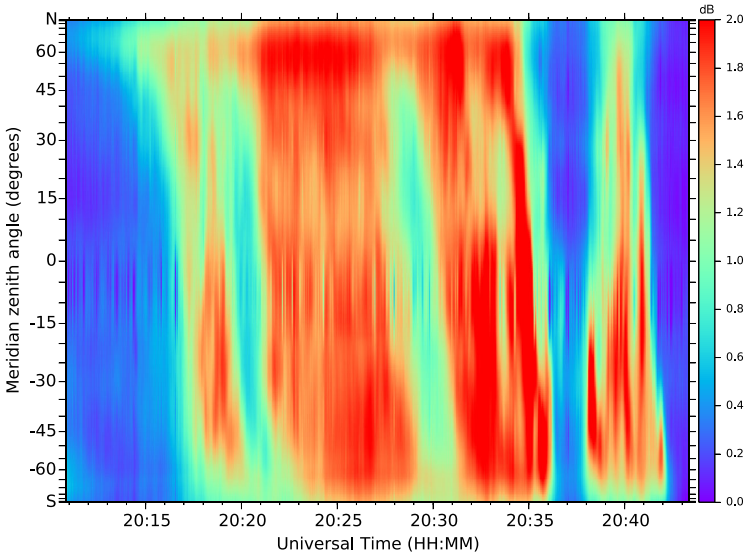

Figure 6. Interferometric riometry keogram at 38.086 MHz showing a 30 min window about the event on the evening of 2 October 2013. The meridional axis is in orthographic projection.

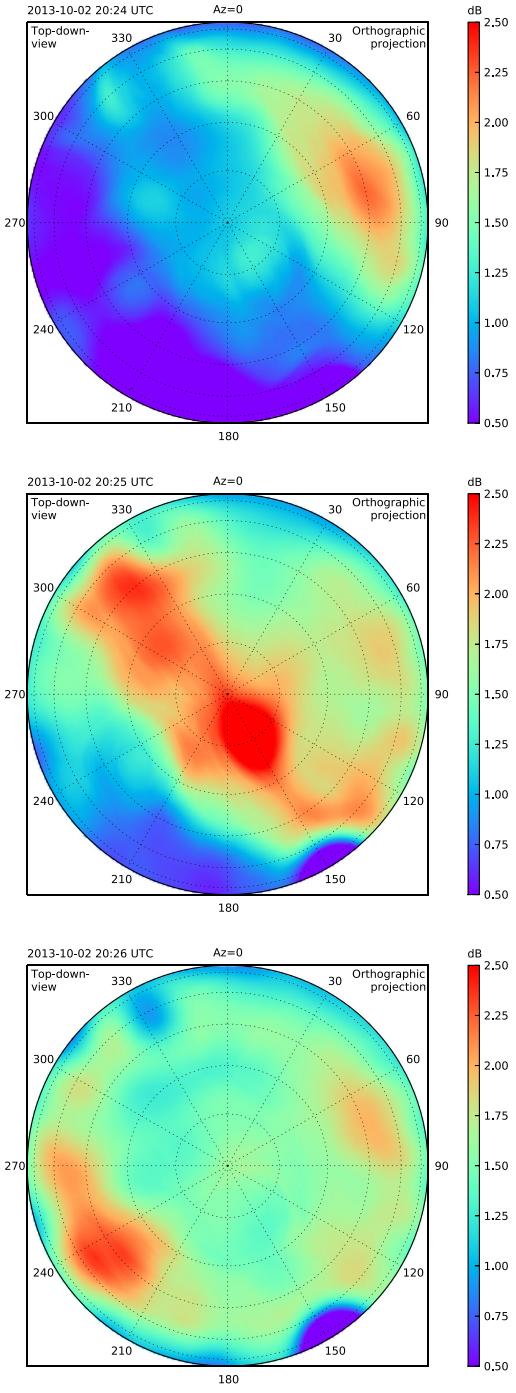

Figure 7. All-sky interferometric riograms at 38.086 MHz, showing the evolution of the evening absorption event.

This method necessitates that the instrument is running for sufficient time before meaningful observations can commence, and also leaves it vulnerable to periods of prolonged geomagnetic disruption. However, these effects need to be taken into account for all riometers and are not particular to the technique described here.

Although sampling and interferometric covariances were taken every second, for the purposes of the summary plots these were combined into 1 min medians in order to reduce the effects of ionospheric scintillation from bright sources (particularly Cas A). This also mitigates the effects of spurious RFI and lessens the volume of data for subsequent processing. The images are already in orthographic projection making display straightforward.

Optical all-sky images of aurorae use a keogram to display only meridian activity as a function of time [e.g., *Eather et al.*, 1976]. For the riometric events, a similar technique is used by producing a 1-D Fourier transform of the meridian pixels ($I_{l,m}$, where $l = 0$) for each time, and then sequencing this into a *riometric keogram*.

3. Results

Interferometric riometry observations commenced on 9 July 2013, with the first observing period continuing until 26 July 2013. A number of minor events were detected during this time but are not discussed in this paper. A second set of measurements was made from 13 September to 7 October 2013 with a major event occurring on the 2 October 2013. This day has been chosen as an example, as there are sufficient features to demonstrate the effectiveness of the technique during complicated events, such as auroral-precipitation-induced absorption. The riometric keogram is shown in Figure 5.

When examining Figure 5, one can see four discrete time periods of auroral-precipitation-induced riometer absorption. The absorption between 3 and 4 UT is very sharp in time, indicating fast-changing high-energy precipitation penetrating deep into the *D* region with largest absorption occurring south of zenith. Between 5 and 7 UT, this is followed by somewhat spatially and temporally structured absorption that migrates northward but has a smaller absorption value and is likely less energetic. Between 12 and 17 UT there is diffuse absorption, probably associated with spatially diffuse, very

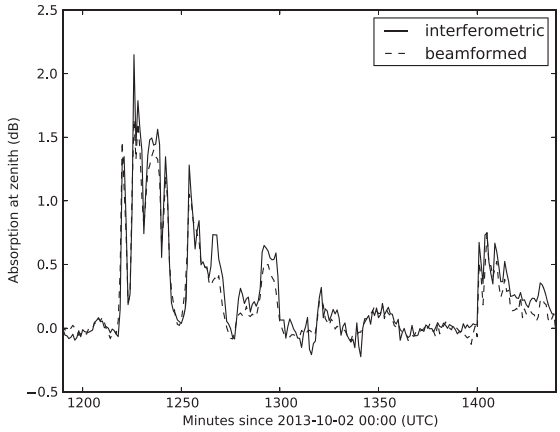

Figure 8. Detail showing the comparison between inteferometric and beamformed absorption measurements.

soft low-energy electron precipitation that is located north, then south, and finally migrates close to zenith. Finally, the last period of absorption occurs between 20:20 and 20:45 UT. Of these events, the evening event shows the most spatial structure and is shown in more detail in Figure 6, which clearly shows that the absorption features appear to migrate in the north-south direction across the field of view, very much in the same way as optical auroral features do.

A few 1 min frames of all-sky interferometric riometry are shown in Figure 7. These reveal the true direction of the arrival of the absorption, sweeping from the northeast to the southwest.

The low-absorption patch centered on Az = 148°, El = 0° is an unidentified RFI source located in the direction of the Kilpisjärvi village. It was emitting during the event which results in positive flux (and thus negative absorption). Although it detracts from that particular sector, the effects on the remainder of the image are minimal. This would not have been the case for a wide beam riometer, whose data would have been completely compromised by the presence of this interference source.

4. Comparisons

To validate the observations, a comparison was made between a KAIRA single-beam riometry result and by one made by taking only the center pixel of the KAIRA interferometric riometry images. The single-beam riometry method is well established, including a comparison to a completely independent technique (incoherent scatter radar [*Kero et al.*, 2014]). The absorption levels from the single-beam and interferometric riometry agree to within 0.2 dB, and a plot showing this comparison for the evening event is shown in Figure 8. The discrepancy can be accounted for by differences in susceptibility to low-level RFI and the omission of zero-spacing baselines in the interferometric case. However, this level of discrepancy does not undermine the technique.

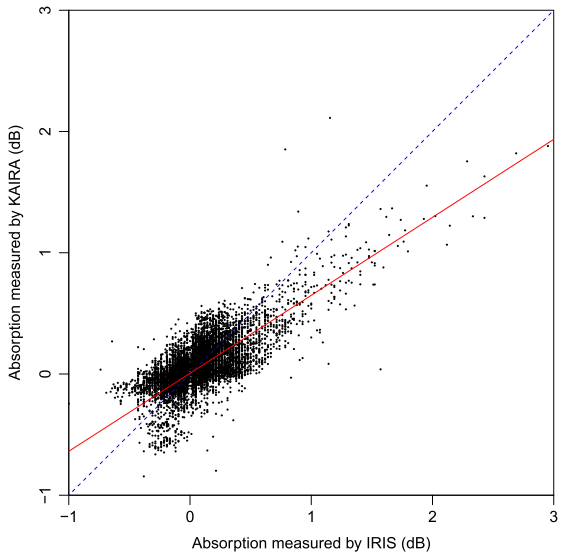

Figure 9. Comparison of all zenith absorption data from 19 October 2014 and 19 March 2015, where KAIRA and IRIS were observing at the same time (556 h total). The dashed line is unity and the solid line is a weighted fit, as explained in the text.

There are no broadbeam riometers in the same region as KAIRA. However, the Imaging Riometer for Ionospheric Studies (IRIS) [*Browne et al.*, 1995] is also located at Kilpisjärvi, Finland (Figure 1) approximately 2.24 km from KAIRA and provides an opportunity to carry out a comparison between the new interferometric riometry technique and the traditional multibeam method. The instruments are of comparable size and have similar beam

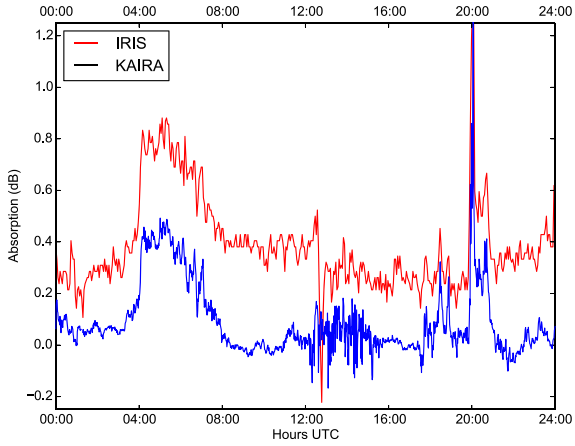

Figure 10. Comparison of a sample 24 h period (30 January 2015).

patterns. The KAIRA LBA array can select any frequency in the 8–80 MHz range and can therefore match the observing frequency of IRIS (38.2 MHz).

A collaboration with the IRIS group has been established and the identification and analysis of mutually observed events are ongoing. Although IRIS was off-line during the event used in this paper to demonstrate the interferometric technique, it has been possible to make a comparison of KAIRA's interferometric technique with the publicly available zenith data from IRIS for the period 19 October 2014 to 19 March 2015. During this time, there were 556 h where cotemporal data from both KAIRA and IRIS were collected, which are plotted against each other in Figure 9.

These observations were automatically processed, rejecting any absorption of magnitude greater than 10 dB. A line of unity (dashed) and a weighted least squares fit (solid) are shown. The weighting, w, used is $\min((A_i^2 + A_k^2)^{\frac{1}{2}}, 1)$, which emphasizes the relationship between stronger absorptions, which correspond to events and are, thus, typically of more interest. The weighted fit gives a slope of 0.54 and intercept of 0.02. The lower value is expected, as this is what has been experienced between the IRIS system which is based on a noise-balancing system compared to the AIRIS system in Andøya which is a digital system and in which beam forming is done via FPGA (similar to KAIRA) [*Honary et al.*, 2011]. This discrepancy remains under investigation.

A sample 24 h period is shown in Figure 10. In this example the median absorption for IRIS is 0.28 dB higher than KAIRA. This nonzero bias in the IRIS data seems to also slowly migrate during the 24 h period. The offset between the data sets is a common feature and contributes to the overall scatter shown in Figure 9. Snow loading (KAIRA has less snow depth than IRIS due to its raised elevation), sensitivity to temperature, and RFI can all contribute to the offset. However, the interferometric system has no zero-length baseline and is therefore less susceptible to such offsets.

5. Discussion

The use of the interferometric method gives many benefits to the riometry application. Apart from achieving an increase in spatial resolution, impossible with single-beam all-sky riometers, it gives continuous all-sky sampling, which is not possible with a multibeam riometer.

The interferometric images are not susceptible to pointing errors. The individual aerial antennas are "all-sky" and the position of the phase tracking center is determined by the observatory clock. Phase accuracy and stability is easy to manage at VHF frequencies. Interferometry is less affected by gain fluctuations on an individual antenna, as long as they are uncorrelated with other antennas. Spectral bandpasses are usually stable for the same reason. And, in anticipation of the application of interferometry to multifrequency riometry, we can adjust the resolution of the map by reweighting the visibilities in software which is useful for combining images from higher frequencies with those from lower frequencies.

As riometry has typically been carried out in the Arctic and Antarctic regions, due to the presence of interesting ionospheric conditions, there is a practical benefit for the use of fixed aerial phased arrays, in that there are no moving parts, which are difficult to protect under extreme environmental conditions. With a large number of antennas, the system is also tolerant of failures of individual elements, as the loss of a few elements has negligible effect on the overall sensitivity and beam pattern and can be easily compensated for as new quiet-sky images are determined. For example, in March 2014 a severe storm resulted in the loss of four polarization channels due to aerial damage but with minimal effect on the data quality.

There are some challenges and limitations associated with interferometric riometry. The data rates are high and the network and signal-processing requirements are demanding for current systems. This will improve with the progression of technology.

Radio bright point sources (such as Cas A) will scintillate, causing large variations in received power. These are easily averaged out for quiet-sky power determination but cannot be directly removed from the observation power without modeling.

Additionally, retaining calibration can be difficult. Snowfalls can affect the antenna response causing day-to-day variation; this is a limitation of the LBA array field design, rather than the interferometric imaging technique. In the event of fast events, such as rain penetrating a layer of snow and radically changing the permittivity, this will cause disruption to the quiet-sky power determination. However, this will be an issue for all antenna designs that do not involve an elevated-and-drained ground screen. There is also an inherent variation between the sidereal diurnal cycle and the solar diurnal cycle, resulting in smearing of the determined quiet-sky power: although the same sidereal time is used throughout the quiet-sky power period, these times are at different solar times and thus have different levels of photoionization. Changes in background ionization also cause day-to-day variations. These effects can be as large as 0.3 dB, with Figure 10 being an example of this. However, the digital interferometric system is less susceptible to such influences.

5.1. Future Work

As KAIRA is based on LOFAR technology, there is a direct compatibility of the KAIRA riometric software with the data acquisition systems of other LOFAR sites. Furthermore, the identical hardware configurations permit a consistency of measurements carried out over a wide area. Cohosting riometry with the astrophysics observations on the same system would be possible due to parallel processing options available on the LOFAR digital system.

Also under consideration is contrasting interferometric riometry measurements with cotemporal optical images of aurorae, allowing for the difference in heights of the two phenomena.

Kero et al. [2014] demonstrate using the KAIRA facility the ability to estimate the ionospheric electron density profile using a selection of observing frequencies ranging from 10 to 80 MHz. The cosmic radio noise absorption observed at multiple frequencies is used to invert the height profile of the electron density by applying a simple parameterized electron precipitation model. This multifrequency riometry is capable of producing realistic electron density profiles under substorm-related electron precipitation conditions. Although the technique in that study uses a multibeam approach, it is also applicable to interferometric riometry. To do this, a multifrequency correlator for KAIRA is planned.

As part of that same development, it is also planned to improve the time resolution of the instrument to achieve rapid sampling; 100samples/s is anticipated. This will permit the study of fast time domain features, which has not been readily possible with existing instruments. The challenge with this will be high data rates, although this is something that advances in computer technology will soon overcome. The authors plan to investigate ionospheric scintillation within riometric images and determine a method to deconvolve the effect of bright point sources.

6. Conclusion

Imaging riometry is a powerful technique as it allows the temporal-spatial study of auroral-induced electron density enhancement. Unlike optical techniques, it is optimal at lower altitudes (*D* region) and the use of VHF radio frequencies means that it can be used during daylight (including the midnight-Sun season) and cloudy conditions.

Using all-sky radio interferometry gives distinct advantages for riometry measurements. The spatial coverage is continuous, preventing uneven areas of sensitivity on the sky—present in multibeam riometers. The interferometric technique reduces the effects of radio frequency interference, as these sources can be localized and thus excised. The same benefit also applies to strongly scintillating sources, such as the cosmic radio sources Cas A and Cyg A.

Since 9 July 2013, KAIRA has been used as an interferometric riometer. The first major absorption event was imaged on 2 October 2013, and the results of those measurements were presented in this paper. This is a significant result as it demonstrates that this technique is a viable and effective means for carrying out detailed spatial analysis of ionospheric opacity.

Acknowledgments
The authors wish to acknowledge A. Kero and M. Brentjens. LOFAR was designed and constructed by ASTRON, Netherlands. KAIRA was funded by the University of Oulu and the FP7 European Regional Development Fund and is operated by Sodankylä Geophysical Observatory. The data used were KAIRA beamlet- and cross-correlation statistics, which are available on request from the KAIRA Observer-in-Charge, Sodankylä Geophysical Observatory, http://www.sgo.fi/KAIRA. The Imaging Riometer for Ionospheric Studies (IRIS) is operated by the Space Plasma Environment and Radio Science (SPEARS) group, Department of Physics, Lancaster University (UK) in collaboration with the Sodankylä Geophysical Observatory. IRIS data are publicly available from http://spears.lancs.ac.uk/iris/. Map data for Figure 1 were drawn with the Generic Mapping Tool, by Wessel and Smith.

References

Browne, S., J. Hargreaves, and B. Honary (1995), An imaging riometer for ionospheric studies, *Electron. Commun. Eng. J.*, *7*(5), 209–217, doi:10.1049/ecej:19950505.
Burke, B. F. (1956), Mills cross telescopes, *Astron. J.*, *61*, 167, doi:10.1086/107300.
Detrick, D. L., and T. J. Rosenberg (1990), A phased-array radiowave imager for studies of cosmic noise absorption, *Radio Sci.*, *25*, 325–338, doi:10.1029/RS025i004p00325.
Eather, R. H., S. B. Mende, and R. J. R. Judge (1976), Plasma injection at synchronous orbit and spatial and temporal auroral morphology, *J. Geophys. Res.*, *81*, 2805–2824, doi:10.1029/JA081i016p02805.
Guzmán A. E., J. May, H. Alvarez, and K. Maeda (2011), All-sky Galactic radiation at 45 MHz and spectral index between 45 and 408 MHz, *Astron. Astrophys.*, *525*, A138, doi:10.1051/0004-6361/200913628.
Hagfors, T., M. Grill, and F. Honary (2003), Performance comparison of cross correlation and filled aperture imaging riometers, *Radio Sci.*, *38*(6), 17–1, doi:10.1029/2003RS002958.
Hargreaves, J. K. (1995), *The Solar-Terrestrial Environment*, Cambridge Univ. Press.
Högbom, J. A. (1974), Aperture synthesis with a non-regular distribution of interferometer baselines, *Astron. Astrophys. Suppl. Ser.*, *15*, 417–426.
Honary, F., S. R. Marple, K. Barratt, P. Chapman, M. Grill, and E. Nielsen (2011), Invited article: Digital beam-forming imaging riometer systems, *Rev. Sci. Instrum.*, *82*(3), 031301, doi:10.1063/1.3567309.
Hysell, D. L., and J. L. Chau (2006), Optimal aperture synthesis radar imaging, *Radio Sci.*, *41*, RS2003, doi:10.1029/2005RS003383.
Kero, A., J. Vierinen, D. McKay-Bukowski, C.-F. Enell, M. Sinor, L. Roininen, and Y. Ogawa (2014), Ionospheric electron density profiles inverted from a spectral riometer measurement, *Geophys. Res. Lett.*, *41*, 5370–5375, doi:10.1002/2014GL060986.
Kudeki, E., and F. Sürücü (1991), Radar interferometric imaging of field-aligned plasma irregularities in the equatorial electrojet, *Geophys. Res. Lett.*, *18*, 41–44, doi:10.1029/90GL02603.
Little, C. G., and H. Leinbach (1959), The riometer—A device for continuous measurement of ionospheric absorption, *Proc. IRE*, *47*, 315–320.
Little, C. G., and A. C. B. Lovell (1950), Origin of the fluctuations in the intensity of radio waves from galactic sources: Jodrell bank observations, *Nature*, *165*, 423–424, doi:10.1038/165423a0.
McKay-Bukowski, D., et al. (2015), KAIRA: The Kilpisjärvi Atmospheric Imaging Receiver Array — system overview and first results, *IEEE Trans. Geosci. Remote Sens.*, *53*, 1440–1451, doi:10.1109/TGRS.2014.2342252.
Ranta, H., and A. Ranta (1977), Study of Latitudinal, Diurnal and Seasonal Variation of Ionospheric Absorption According to Observations of the Riometer Network in Finland, vol. 14.
Roger, R. S., C. H. Costain, T. L. Landecker, and C. M. Swerdlyk (1999), The radio emission from the Galaxy at 22 MHz, *Astron. Astrophys.*, *137*, 7–19, doi:10.1051/aas:1999239.
Ryle, M., and A. Hewish (1950), The effects of the terrestrial ionosphere on the radio waves from discrete sources in the galaxy, *Mon. Not. R. Astron. Soc.*, *110*, 381.
Ryle, M., A. Hewish, and J. Shakeshaft (1959), The synthesis of large radio telescopes by the use of radio interferometers, *IEEE Trans. Antennas Propag.*, *7*, 120–124, doi:10.1109/TAP.1959.1144745.
Shain, C. A. (1951), Galactic radiation at 18.3 Mc/s., *Aust. J. Sci. Res. Phys. Sci.*, *4*, 258–267.
Thompson, A. R. (1999), Fundamentals of radio interferometry, in *Synthesis Imaging in Radio Astronomy II*, edited by G. B. Taylor, C. L. Carilli, and R. A. Perley, *Astron. Soc. of the Pac. Conf. Ser.*, *180*, 11–36
van Cittert, P. H. (1934), Die Wahrscheinliche Schwingungsverteilung in Einer von Einer Lichtquelle Direkt Oder Mittels Einer Linse Beleuchteten Ebene, *Physica*, *1*, 201–210, doi:10.1016/S0031-8914(34)90026-4.
van Haarlem, M. P., et al. (2013), Lofar: The low-frequency array, *Astron. Astrophys.*, *556*(A2), 53, doi:10.1051/0004-6361/201220873.
Virtanen, I. I. (2012), Station Data Cookbook.
Woodman, R. F. (1971), Inclination of the geomagnetic field measured by an incoherent scatter technique, *J. Geophys. Res.*, *76*, 178–184, doi:10.1029/JA076i001p00178.
Zernike, F. (1938), The concept of degree of coherence and its application to optical problems, *Physica*, *5*, 785–795, doi:10.1016/S0031-8914(38)80203-2.